



CHORUS

This is the accepted manuscript made available via CHORUS. The article has been published as:

Waves in a quasi-two-dimensional superparamagnetic dusty plasma liquid in a trap

M. Rosenberg, Gabor J. Kalman, P. Hartmann, and Z. Donkó

Phys. Rev. E **94**, 033203 — Published 6 September 2016

DOI: [10.1103/PhysRevE.94.033203](https://doi.org/10.1103/PhysRevE.94.033203)

Waves in a quasi-two-dimensional superparamagnetic dusty plasma liquid in a trap

M. Rosenberg

*Department of Electrical and Computer Engineering,
University of California San Diego, La Jolla CA 92093*

Gabor J. Kalman

Department of Physics, Boston College, Chestnut Hill, MA 02467

P. Hartmann and Z. Donkó

*Institute for Solid State Physics, Wigner Research Centre for Physics,
Hungarian Academy of Sciences, H-1525 Budapest, P.O. Box 49, Hungary and
Department of Physics, Boston College, Chestnut Hill, MA 02467*

In a two-dimensional dusty plasma composed of superparamagnetic, charged dust grains and immersed in an external magnetic field \mathbf{B} , the grains interact via both Yukawa and magnetic dipole-dipole potentials. Because the grains' magnetic dipole moments are induced by \mathbf{B} , the dipole moments all lie along \mathbf{B} . When \mathbf{B} is tilted with respect to the normal to the dust layer, the interaction between the grains becomes anisotropic. In our previous paper (Hartmann *et al.*, 2014, *Phys. Rev. E* **89**, 043102) we studied the character of waves in such a system, confined strictly to two dimensions, without any spatial extension in the direction perpendicular to the layer. We analyzed how the dispersion of waves depends on the direction of propagation and the relative strengths of the magnetic dipole and Yukawa potentials. In this paper, we consider a more realistic quasi-2D system where the grains are confined by an external potential and can undergo small oscillations perpendicular to the layer. We analyze the effect of the strength of the confining potential on the in-plane correlations and on the wave propagation. In addition to the in-plane compressional and transverse waves, there now appears an out-of-plane transverse wave generated by the oscillation of the grains in the confining potential. The theoretical approach uses the Quasi-Localized Charge approximation paralleled by molecular dynamics simulations.

I. INTRODUCTION

Dusty plasmas contain small (micron sized) charged solid particulates, or dust grains. Because the dust grains can be imaged, collective processes such as the behavior of dust waves can be observed on the kinetic particle level. Typically the dust grains interact via a screened Coulomb (Yukawa) interaction, where the dust charge is screened by the background electrons and ions. When the Yukawa potential energy is larger than the thermal (kinetic) energy of the dust, the dust is strongly coupled [1–3]. The behavior of dust waves in weakly or strongly coupled dusty plasmas have been studied theoretically and experimentally (e.g., [4–11]). Generally in terrestrial laboratory experiments, waves in two-dimensional (2D) layers of strongly coupled dust grains have been studied, owing to the difficulty of generating 3D systems due to gravitational compression.

With the advent of experiments on dusty plasmas immersed in large magnetic fields (e.g., [12] and refs. therein), there has been interest in collective processes involving grains with magnetic properties that interact via magnetic dipole forces in addition to Yukawa forces (e.g., [13–17]). Recently, we theoretically investigated wave behavior in the liquid phase of a 2D dusty plasma composed

of superparamagnetic grains and immersed in an external uniform magnetic field \mathbf{B} whose magnitude and direction with respect to the layer could be varied ([16], to be referred to as I in the sequel). Since the grains acquire a magnetic dipole moment along \mathbf{B} , the magnetic dipole moments are parallel. When \mathbf{B} is normal to the layer, the dipole interaction is repulsive. When \mathbf{B} is tilted with respect to the layer, the magnetic dipole interaction becomes anisotropic. It also becomes attractive along the projection of \mathbf{B} in the layer if the angle α between \mathbf{B} and the layer is smaller than a threshold angle α_{th} , while it is repulsive otherwise. We studied wave dispersion for $\alpha > \alpha_{th}$ which would correspond to stable equilibrium. It was found that two modes can propagate in the layer, corresponding to a compressional and transverse mode at small wavenumber k . The wave dispersions depend on the ratio of the strengths of the magnetic dipole to Yukawa interactions, and the direction of propagation in the layer when $\alpha \neq 90^\circ$.

In an experiment, one may expect that the grain layer would be confined by an external potential normal to the layer. In this paper, we extend our prior analysis in I to include the effects of the confining potential and allow the dust grains to have small oscillations perpendicular to the layer. Similarly to the magnetic field-free quasi-2D

Yukawa system [18], there is a new out-of-plane transverse mode in this system generated by the oscillation of the grains in the confining potential with a frequency that is determined primarily by the strength of the confining potential.

Our theoretical approach uses the Quasi-Localized Charge Approximation (QLCA) reformulated to treat dipole interactions [16, 19–21]. Paralleling the theoretical analysis we have performed Molecular Dynamics (MD) simulations of the system. The simulation generates fluctuation spectra, which provide the basis for comparison with the QLCA collective mode spectrum. The simulations also provide the pair correlation function which is needed as input for the QLCA calculations.

A goal of this study is to try to motivate experiments in waves in 2D dusty plasmas where the dust interacts via tunable anisotropic potentials. While the present system involves paramagnetic grains, the study may also have relevance to understanding the behavior of waves in other systems where the particles interact via dipole interactions. This may include, for example, 2D dusty plasmas with induced electric dipole interactions (i.e., “electrorheological” dusty plasmas [22, 23]) and 2D dipolar bosonic gases with tilted magnetic or electric dipoles [24].

The paper is organized as follows. Section II describes the model system. Section III presents the theoretical approach using the QLCA and discusses the MD simulations. Section IV presents results for the mode dispersion relations. Section V gives a summary.

II. MODEL SYSTEM

The model system is a quasi-2D layer in a harmonic trap, composed of charged superparamagnetic dust grains of uniform size and material properties in a plasma immersed in a constant, homogeneous external magnetic field \mathbf{B} . Each grain has a mass m_d , a negative electric charge Q and an induced magnetic dipole moment \mathbf{M} along \mathbf{B} . The dust areal density in the layer is given as $n_d = 1/\pi a^2$, where a is the Wigner-Seitz radius. It is assumed that the grains are strongly coupled in the liquid phase. The dust layer is centered in the $x - y$ plane, with a very small but finite width in the z -direction. The magnetic field makes an angle α with respect to the layer. Without loss of generality, we take the x -axis to be the direction of the projection of \mathbf{B} in the plane, so that the magnetic moment of each dust grain lies in the $x - z$ plane, as shown in Fig. 1. In our analysis, we will consider waves that propagate in the $x - y$ plane, with the direction of propagation being defined by the angle χ between the wavevector \mathbf{k} and the x -axis.

The grains interact via Yukawa and magnetic dipole-dipole potentials. The Yukawa interaction energy between two grains with charge Q separated by a distance r is

$$\phi_Y = \frac{Q^2}{r} e^{-r/\lambda_D}, \quad (1)$$

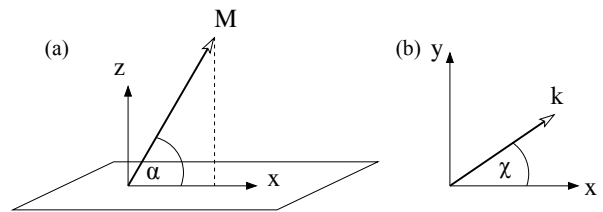


FIG. 1. (a) The dust layer is centered in the $x - y$ plane, and the magnetic moment \mathbf{M} of each grain lies in the $x - z$ plane, at an angle α with respect to the x -axis. (b) The angle between the wavevector, which lies in the $x - y$ plane, and the x -axis is χ .

where λ_D is the plasma Debye screening length. The magnetic dipole-dipole interaction energy is [13, 25]

$$\phi_M = \frac{M_\mu M_\nu}{r^3} \left(\delta_{\mu\nu} - 3 \frac{\mu\nu}{r^2} \right), \quad (2)$$

where $\mu, \nu = x, y, z$. It is assumed that the only effect of the magnetic field on the dust grains is via the induced dipole-dipole force, that is, that the grain motion is not affected by Lorentz forces.

The Yukawa force between the like-charged particles,

$$\mathbf{F}_Y(r) = -\frac{\partial \phi_Y}{\partial r} \frac{\mathbf{r}}{r} = \frac{Q^2}{r^2} e^{-r/\lambda_D} \left(1 + \frac{r}{\lambda_D} \right) \frac{\mathbf{r}}{r}, \quad (3)$$

is always repulsive. However, the magnetic dipole-dipole force for the system shown in Fig. 1,

$$\mathbf{F}_M(r) = \frac{3M^2}{r^4} \left[\frac{\mathbf{r}}{r} \left(1 - 5 \frac{(x \cos \alpha + z \sin \alpha)^2}{r^2} \right) + 2\mathbf{m} \frac{(x \cos \alpha + z \sin \alpha)}{r} \right]. \quad (4)$$

can be repulsive or attractive depending on the relative positions and orientations of the grains. In (4), the vector $\mathbf{m} = (\cos \alpha, 0, \sin \alpha)$ is the unit vector pointing along the direction of the dipole.

In addition to these two forces, it is assumed that the dust layer is confined in the z -direction by a harmonic potential whose strength is characterized by the parameter t ,

$$V_z = \frac{t^2 z^2}{2} \omega_{pd}^2 m_d, \quad (5)$$

leading to the confinement force

$$F_{Cz} = -t^2 \omega_{pd}^2 m_d z, \quad (6)$$

where ω_{pd} is the dust plasma frequency, given by $\omega_{pd}^2 = 2\pi Q^2 n_d / m_d a$.

The effect of the confining potential is to counteract the tendency of the grains to escape from the layer. In addition, the magnetic dipole-dipole force can become attractive for certain combinations of α and displacements

in the z -direction, resulting in possible instabilities. In this analysis we wish to avoid such situations, and will only consider the parameter space where we expect the magnetic dipole-dipole force would be repulsive.

To get an idea of this parameter space, we consider the system shown in Fig. 1 in cylindrical co-ordinates where $x = \rho \cos \theta$ and $y = \rho \sin \theta$, where θ is the polar angle in the dust layer plane, measured from the x -axis. We expect F_M would be softest in the $x - z$ plane (i.e., $\theta = 0$) since this is the plane of \mathbf{M} . When \mathbf{r} is purely in the x -direction, the x component of the magnetic dipole force is $F_{Mx} = (3M^2/r^4)[1 - 3\cos^2 \alpha]$. For α smaller than a threshold angle $\alpha_{th} = \cos^{-1}(1/\sqrt{3}) \approx 54.74^\circ$, the magnetic dipole force becomes attractive in this direction. Thus, as in paper I we restrict the analysis to magnetic tilt angles larger than α_{th} . Now, when \mathbf{r} has a small component z ($\ll x$) in the z -direction, we have $F_{Mx} \approx (3M^2/r^4)[(1 - 5f^2) + 2f \cos \alpha]$, where $f \approx \cos \alpha + (z/r) \sin \alpha$. This leads to a condition on z/r in order that F_{Mx} remains repulsive. For example, when $\alpha = 60^\circ$, the condition for $F_{Mx} > 0$ is roughly that $z/r < .067$. It may be noted that when z/r is small, the z -component of the magnetic dipole force F_{Mz} is repulsive and tends to increase in magnitude as α decreases toward α_{th} . The requirement that the particle displacement in the z -direction is small compared to the spacing in $x - y$ plane may be controlled by the strength t^2 of the confining potential, as will be discussed in the next section.

The model system is thus described by a set of parameters that characterize the Yukawa interaction, the magnetic dipole interaction, and the confining potential. The Yukawa interaction is characterized by the Coulomb coupling parameter $\Gamma = Q^2/ak_B T_d$ and a screening parameter $\kappa = a/\lambda_D$ (here k_B is the Boltzmann constant, and $k_B T_d$ is the thermal or kinetic energy of the grains). We use the quantity $\eta = M/Q\lambda_D$ as a measure of the strength of the magnetic dipole-dipole compared to the electrostatic Yukawa interaction. Finally, the parameter t^2 characterizes the strength of the confining potential.

III. THEORETICAL/COMPUTATIONAL APPROACH

The theoretical methodology uses the QLCA combined with MD simulations, which has been successfully applied to describe waves in various strongly coupled Yukawa systems in the liquid phase [26, 27], including recently waves in 2D superparamagnetic dusty plasma liquids [16]. Here, we use a reformulated QLCA which can treat dipole interactions [19–21]. For our system, we take the magnetic dipole-dipole and Yukawa interactions to be additive. We allow the grains to have small oscillations in the z -direction under the influence of the confining potential and the forces originating from the other particles in the layer.

The QLCA mode dispersion relations are given by (see

I)

$$\begin{vmatrix} \omega^2 - C_{xx} & C_{xy} & C_{xz} \\ C_{yx} & \omega^2 - C_{yy} & C_{yz} \\ C_{zx} & C_{zy} & \omega^2 - C_{zz} - t^2 \omega_{pd}^2 \end{vmatrix} = 0, \quad (7)$$

where $C_{\mu\nu}(\mathbf{k})$ is the QLCA dynamical matrix,

$$C_{\mu\nu}(\mathbf{k}) = -\frac{n}{m_d} \int d^2r d\theta g(r, \theta) [\exp(i\mathbf{k} \cdot \mathbf{r}) - 1] \partial_\mu \partial_\nu \phi_{Tot}. \quad (8)$$

Here, $g(r, \theta)$ is the equilibrium 2D pair correlation function between the particles in the layer projected onto the center plane, and ϕ_{Tot} is the sum of the Yukawa potential (1) and the magnetic dipole-dipole interaction potential (2). The term $t^2 \omega_{pd}^2$ in the zz element of the matrix in (7) comes from harmonic motion of the dust in the confining potential, (see eq. 6), which leads to what we will call a “trap frequency” due to the confining potential, given by $\omega_t = t\omega_{pd}$.

In the theoretical treatment it is assumed that the vector \mathbf{r} between grains in the dust layer of finite width is well approximated by its projection onto the center plane and is given by $\mathbf{r} = \rho(\cos \theta, \sin \theta, 0)$. That is, we assume that the dust layer is of negligible thickness and that the precise structure of the density profile along the z -direction would not affect the dispersion. In a more faithful model one would retain \mathbf{r} as a 3-dimensional vector and would integrate along the z -direction, using the measured density profile (cf. Fig. 10). Due to the smallness of the width of the layer, the approximation we use should not lead to a significant error in the calculation.

We write the components of the dynamical matrix using the quantities $\bar{k} = ka$, $\bar{r} = r/a$ (with $\bar{\mu}, \bar{\nu} = \bar{x}, \bar{y}$ as discussed in the previous paragraph), $\bar{\kappa} = a/\lambda_D$ and $\eta = M/Q\lambda_D$. With the angle between \mathbf{k} and the x -axis taken as χ , the angle between \mathbf{k} and \mathbf{r} is given by $(\chi - \theta)$. Then $C_{\mu\nu}$, which is a function of parameters α , Γ , κ , η and t , can be written as

$$\begin{aligned} C_{\mu\nu}(\mathbf{k}) = & \frac{\omega_p^2}{2\pi} \int d\theta \frac{d\bar{r}}{\bar{r}^2} g(\bar{r}, \theta) [\exp(i\bar{k}\bar{r} \cos(\chi - \theta)) - 1] \\ & \times \left\{ \exp(-\bar{\kappa}\bar{r}) \left[(1 + \bar{\kappa}\bar{r}) \left(\delta_{\mu\nu} - 3\frac{\bar{\mu}\bar{\nu}}{\bar{r}^2} \right) - \frac{\bar{\mu}\bar{\nu}}{\bar{r}^2} \bar{\kappa}^2 \bar{r}^2 \right] \right. \\ & + \frac{3\eta^2}{\bar{\kappa}^2 \bar{r}^2} \left[\left(\delta_{\mu\nu} - 5\frac{\bar{\mu}\bar{\nu}}{\bar{r}^2} \right) - 5\cos^2 \alpha \cos^2 \theta \left(\delta_{\mu\nu} - 7\frac{\bar{\mu}\bar{\nu}}{\bar{r}^2} \right) \right. \\ & \left. \left. - 10\cos \alpha \cos \theta \left(m_\mu \frac{\bar{\nu}}{\bar{r}} + m_\nu \frac{\bar{\mu}}{\bar{r}} \right) + 2m_\mu m_\nu \right] \right\}. \quad (9) \end{aligned}$$

The elements of the dynamical matrix $C_{\mu\nu}$ are given explicitly in the Appendix.

We will solve (7) using (9) to obtain the QLCA mode dispersions for arbitrary wavenumber k for waves propagating in the $x - y$ plane. To evaluate (9) requires input of the equilibrium pair correlation function $g(r, \theta)$ which is obtained by MD simulations.

Our molecular dynamics code is an extended version of the code that we have used for our studies of

two-dimensional superparamagnetic dusty plasma liquids [16]. Here we also simulate the motion of $N = 5000$ point-like particles within a square box (with a side length of approximately $L = 125a$) with periodic boundary conditions. Now, small displacements of the particles in the z direction are also allowed, but constrained by a parabolic confinement potential. The spatial fast decay of the interaction forces makes it possible to introduce a cutoff distance, beyond which the interaction of particle pairs can be neglected when the forces acting on the particles are calculated. For our conditions $r_{\text{cutoff}} \cong 30a$. The integration of the equations of motion is performed with the velocity-Verlet scheme. At the initialization of the simulations the positions of the particles are set randomly around the center plane, but according to a canonical distribution function for the system in the confining potential along the z -direction, corresponding to a specified system temperature. The initial velocity vectors are sampled from a Maxwellian distribution corresponding to the same system temperature. During the first phase of the simulations particle velocities are rescaled in each time step, in order to reach the desired temperature. This procedure is stopped before the data collection takes place, where the stability of the simulation is confirmed by monitoring the temperature as a function of time. In the measurement phase of the simulation data are collected for the pair correlation function and for the spatial Fourier components of the microscopic currents in different directions in the x - y plane, as well as in the perpendicular, z -direction, which yield, after an additional Fourier transform in the time domain, the spectra of the current-current correlations.

Due to the peculiarities of the magnetic dipole interactions and to the excursions of the particles from the x - y plane no absolute stability of the system is guaranteed as certain particle arrangements result in strong attraction and diverging forces between certain pairs. In reality a softening of the potential at small distances, or a finite size for the particles would prevent the development of this instability. Since neither of these features is introduced in the model, the simulation cannot handle these cases. At reasonably strong confinement potentials, however, the occurrence of such scenarios is very rare, and long times can be simulated without issues of stability.

IV. RESULTS

In this section we present results for the wave dispersion relations using the QLCA and compare the QLCA results with the mode dispersions obtained from the fluctuation spectra generated by the simulations.

Figure 2 shows polar diagrams of the equilibrium 2D pair correlation functions $g(\bar{r}, \theta)$ along with the corresponding $g(\bar{r})$ in the x , y and *diagonal* directions for a dust layer with $\bar{\kappa} = 1$, $\Gamma = 100$, $\alpha = 60^\circ$ and combinations of η and the trapping frequency parameter t . Since η is finite, the pair correlation functions are anisotropic

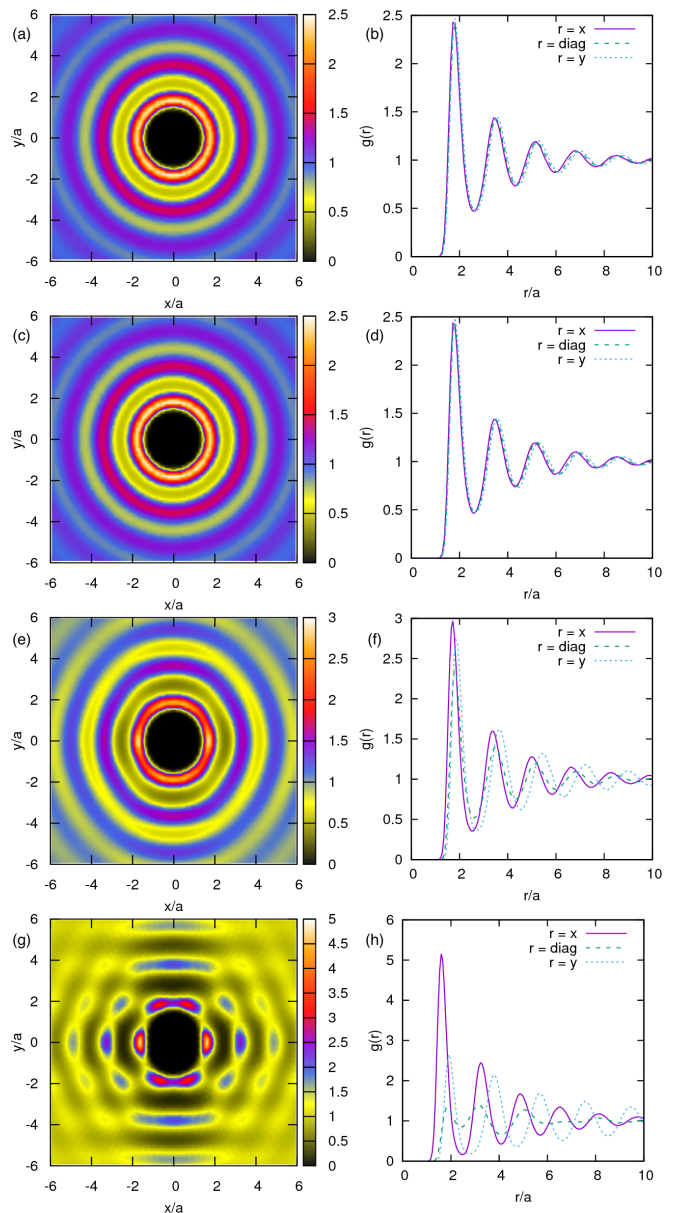


FIG. 2. (Color online) Equilibrium 2D pair correlation function $g(\bar{r}, \theta)$ in the dust layer and corresponding $g(\bar{r})$ in the x -direction (purple, solid curve), the $\theta = 45^\circ$ diagonal direction (green, dashed curve) and y -direction (blue, dotted curve). Parameters are $\bar{\kappa} = 1$, $\Gamma = 100$ and $\alpha = 60^\circ$, with (a-b) $\eta = 0.2$, $t = 1$ (c-d) $\eta = 0.2$, $t = 2$, (e-f) $\eta = 0.4$, $t = 2$ and (g-h) $\eta = 0.7$, $t = 6$. Note the remarkable weakening of correlations along the diagonal direction.

in the plane, though only mildly so for small $\eta = 0.2$ in Figs. 2(a-b) and 2(c-d). As can be seen by comparing the latter two sets of figures, there is very little effect on $g(\bar{r}, \theta)$ due to the confining potential. The effect of increasing η can be seen by comparing Figs. 2(c-d) and 2(e-f) at fixed t , which shows that as η increases, the total interaction potential becomes more anisotropic in the plane. Because the magnetic dipole interaction is most

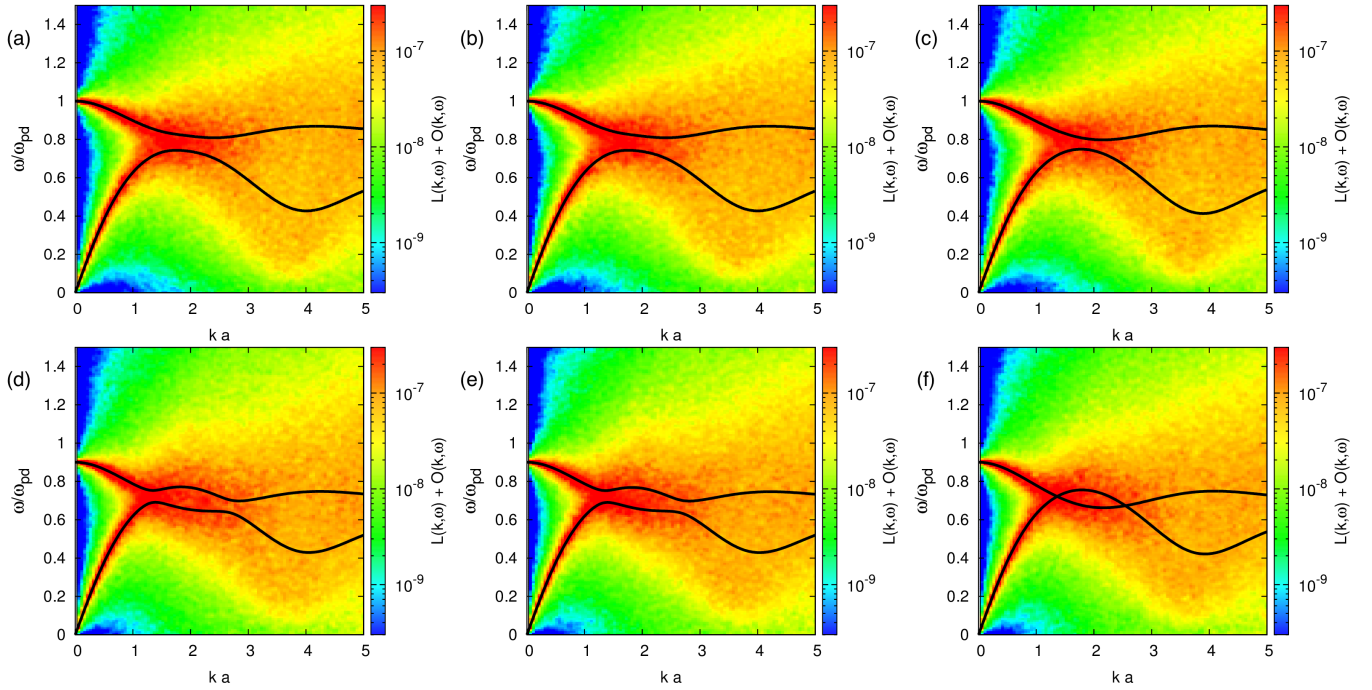


FIG. 3. (Color online) Wave dispersions for the in-plane longitudinal and out-of-plane transverse modes, for several propagation angles for a system with $\Gamma = 50$, $\kappa = 1$, $\alpha = 60^\circ$, $\eta = 0.2$. The trap frequency is $\omega_t = \omega_{pd}$ in (a-c) and $\omega_t = 0.9\omega_{pd}$ in (d-f). The color maps are the in-plane longitudinal and out-of-plane transverse fluctuation spectra generated by the simulations. The curves are the QLCA wave dispersion relations for the corresponding modes obtained from eq. (7) as a function of ka for these parameters. (a, d) $\chi = 0^\circ$, (b, e) $\chi = 30^\circ$, (c, f) $\chi = 90^\circ$. Note the hybridization of the two modes for the weaker trapping frequency.

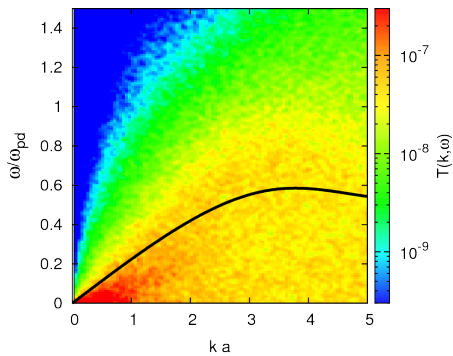


FIG. 4. (Color online) Wave dispersion for the transverse in-plane mode. The color map is the in-plane transverse fluctuation spectrum generated by the simulations for a system with the same parameters as in Fig. 3(a). The curve is the QLCA wave dispersion relation for this mode obtained from eq. (7) as a function of ka .

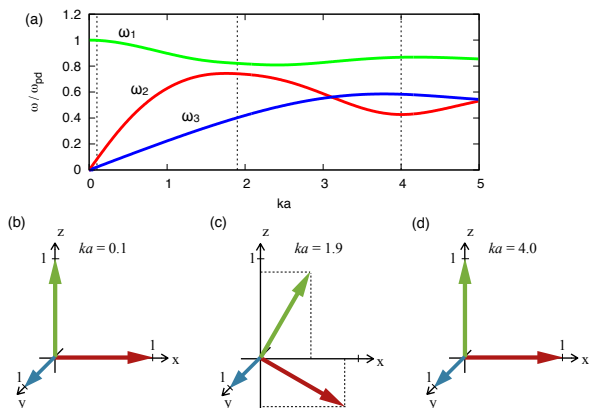


FIG. 5. Polarization of the three QLCA eigenmodes obtained from diagonalizing (9). Parameters are the same as in Fig. 3(a). Green corresponds to the out-of-plane mode (ω_1), red to the in-plane longitudinal mode (ω_2) and blue to the in-plane transverse mode (ω_3). (a) The 3 QLCA modes vs. ka . Polarization vectors of the 3 modes at (b) $ka = 0.1$, (c) $ka = 1.9$ and (d) $ka = 4.0$.

repulsive in the y -direction, the dust particle spacing increases in this direction. Since the dust areal density is constant, the dust particles rearrange themselves so that spacings in the x -direction decrease somewhat in the $\eta = 0.4$ case compared to the $\eta = 0.2$ case. This effect is more pronounced in Figs. 2(g-h) which show a case with $\eta = 0.7$, with $t = 6$ the structure here has a tendency to develop stripe-like density distributions along the x direction, with a remarkable emptying effect along the diagonal. (This behavior may be compared with the similar behavior exhibited by the 2D layer [I, Fig. 2]).

With the dust grains allowed to have small oscillations perpendicular to the dust layer under the influence of the confining potential, a new out-of-plane polarized transverse mode appears, in addition the two in-plane modes considered in our prior paper I. The out-of-plane mode

has been analyzed for a quasi-2D pure Yukawa liquid by Donko et al. [18]. This mode has a finite frequency at $k = 0$, which we refer to as the trap frequency $\omega_t = t\omega_{pd}$, which corresponds the entire layer oscillating in unison in the potential well [26]. In the $k \rightarrow \infty$ limit, the mode frequency becomes the Einstein frequency for this polarization, i.e., the oscillation frequency of a single particle in the frozen environment of the rest of the system. The Einstein frequency is always lower than the trap frequency: the difference is due to the depolarizing effect of the grains (i.e., the grains generate a field which opposes the trapping field). Our earlier comment concerning the density profile along z should be, however, kept in mind: the depolarization effect predicted here would be altered by a self-consistent calculation based on the measured density profiles (Fig. 10). The following will consider the behavior of the three modes in this system.

Figure 3 shows the behavior of the wave dispersions as a function of propagation angle χ , for an anisotropic system with $\alpha = 60^\circ$, $\Gamma = 50$, $\kappa = 1$, $\eta = 0.2$, and trap frequency $\omega_t = \omega_{pd}$ (top row) and $\omega_t = 0.9\omega_{pd}$ (bottom row). In each figure, the upper curve corresponds to the QLCA out-of-plane transverse mode, while the lower curve corresponds to the QLCA in-plane longitudinal mode. The QLCA modes are superimposed on the longitudinal in-plane and transverse out-of-plane fluctuation spectra generated by the simulations. Figure 4 shows just the transverse QLCA in-plane mode superimposed on the transverse in-plane fluctuation spectra generated by the simulations for the same parameters as in Fig. 3(a).

As can be seen from Fig. 3, there is a tendency for the hybridization of the out-of-plane transverse wave with the in-plane longitudinal wave at a certain interval of ka values as the predicted dispersion curves approach each other. In fact, the simulation data show a complete merging of the two modes in this interval. Because the maximum frequency of the longitudinal mode increases as χ increases (due to an increase of strength of the repulsive magnetic dipole interaction in the plane, see I), this effect becomes more pronounced at $\chi = 90^\circ$.

The eigenvectors of the dynamical matrix $C_{\mu\nu}$ determine the polarization of the 3 modes. Figure 5 shows the corresponding polarization vectors for the parameters of Fig. 3(a), for propagation angle $\chi = 0^\circ$, at particular wavenumbers ka . As pointed out above, in the hybridization region at $ka = 1.9$, the polarizations of the out-of-plane (ω_1) and longitudinal in-plane (ω_2) modes become mixed, with polarization vector components in both x and z -directions. On the other hand, the transverse in-plane (ω_3) mode remains largely transverse with polarization vector in the y -direction. As discussed in our prior paper I, the polarizations of the in-plane modes can also become mixed at larger ka where the frequencies of these modes approach each other, although in general, the respective longitudinal and transverse polarizations prevail for small k [28, 29].

Figure 6 shows how the relative strength of the mag-

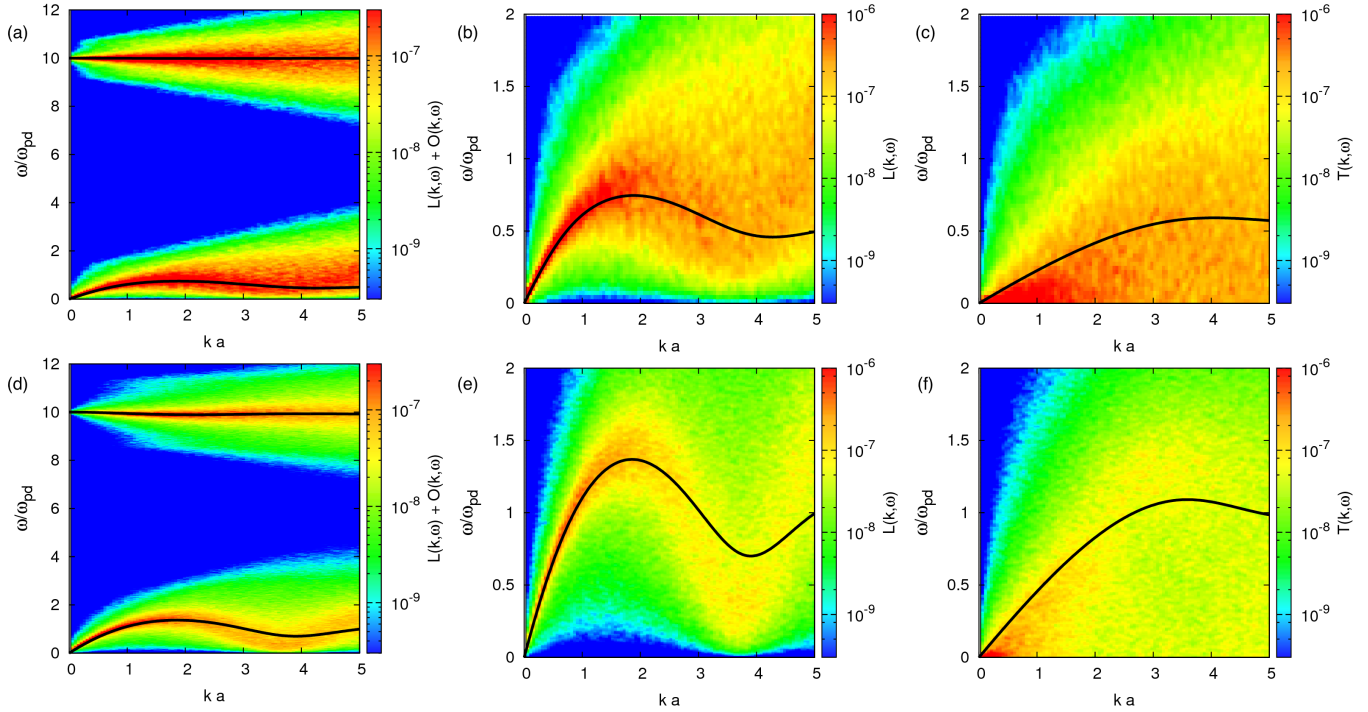


FIG. 6. (Color online) Wave dispersions for the in-plane longitudinal and out-of-plane transverse modes, showing the effect of the magnetic field, with $\eta = 0$ (a-c) and $\eta = 1$ (d-f) for a system with parameters $\Gamma = 25$, $\kappa = 1$, $\alpha = 90^\circ$, $\chi = 0^\circ$, and trap frequency $\omega_t = 10\omega_{pd}$. The color maps in (a) and (d) are the in-plane longitudinal and out-of-plane transverse fluctuation spectra generated by the simulations, and the curves are the QLCA wave dispersion relations for the corresponding modes obtained from eq. (7) as a function of ka for these parameters. The color maps in (b) and (e) [(c) and (f)] are the in-plane longitudinal [transverse] fluctuation spectra, and the curves are the QLCA dispersion relations for the corresponding modes.

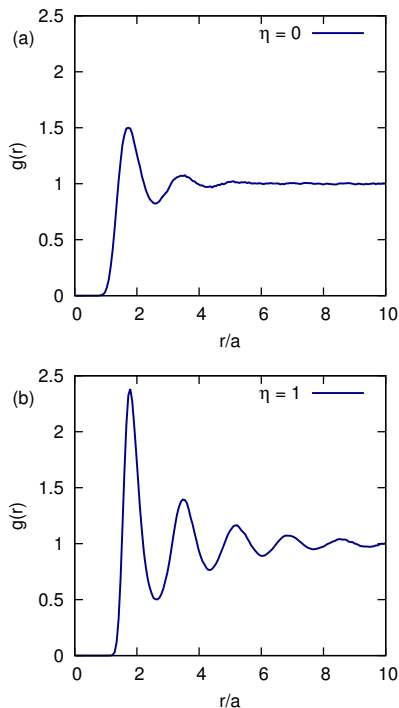


FIG. 7. (Color online) Equilibrium pair correlation functions showing the effect of the magnetic field, for the same parameters as in Fig. 6, and for (a) $\eta = 0$ and (b) $\eta = 1$.

netic dipole interaction, characterized by η , affects the mode dispersions for a system with $\Gamma = 25$, $\kappa = 1$, $\alpha = 90^\circ$, $\chi = 0^\circ$ and trap frequency $\omega_t = 10\omega_{pd}$. Figures 6(a-c) show results for $\eta = 0$ corresponding to the Yukawa liquid, while Figures 6(d-f) show results for $\eta = 1$. In Figure 6(a) and 6(d), the QLCA curves for the corresponding modes are superimposed on the fluctuation spectra for the in-plane longitudinal mode and the out-of-plane transverse mode generated by the simulations. The QLCA dispersion curves for the corresponding in-plane polarized modes are superimposed on the fluctuation spectra for the in-plane longitudinal mode in Fig. 6(b) and 6(e), and the in-plane transverse mode in Fig. 6(c) and 6(f). It can be seen from Fig. 6 that for η different from zero, the maximum frequencies of the in-plane longitudinal and transverse waves increase because the magnitude of the total repulsive inter-grain potential increases. In addition, the difference in the maximum frequency and first dip in the dispersion of the in-plane longitudinal mode is more pronounced for finite η . The effect of the magnetic dipole interaction is also reflected in the behavior of the pair correlation function shown in Figure 7, which shows a stronger localization of the particles owing to the stronger repulsive potential as η increases.

A comparison of the dispersion curves in Figures 8 and 9 illustrate how the tilt angle α of the external magnetic field influences the wave dispersion relations in a system with $\Gamma = 25$, $\kappa = 1$, $\eta = 1$, and trap frequency

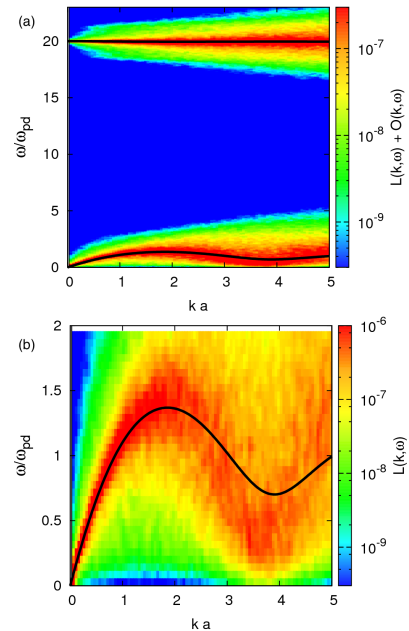


FIG. 8. (Color online) Wave dispersions for the in-plane longitudinal and out-of-plane transverse modes, showing the effect of a strong trap, with trap frequency $\omega_t = 20\omega_{pd}$, for a system with parameters $\Gamma = 25$, $\kappa = 1$, $\alpha = 90^\circ$, $\chi = 0^\circ$, and $\eta = 1$. The color maps in (a) are the in-plane longitudinal and out-of-plane transverse fluctuation spectra generated by the simulations, and the curves are the QLCA wave dispersion relations for the corresponding modes obtained from eq. (7) as a function of ka for these parameters. The color map in (b) is the in-plane longitudinal fluctuation spectra, and the curve is the QLCA dispersion relation for this mode.

$\omega_t = 20\omega_{pd}$. Figure 8 shows results for $\alpha = 90^\circ$ while Figure 9 shows results for $\alpha = 60^\circ$. Since the mode dispersions do not depend on the propagation angle χ when $\alpha = 90^\circ$, only the case of $\chi = 0^\circ$ is shown in Fig. 8. Figure 8(a) shows QLCA curves for the corresponding modes superimposed on the fluctuation spectra for the in-plane longitudinal mode and the out-of-plane transverse mode generated by the simulations. Figure 8(b) shows the QLCA dispersion curves for the in-plane longitudinal mode superimposed on the fluctuation spectra. Figure 9 shows similar mode dispersion graph formats as in Fig. 8, but for several different propagation angles for the anisotropic case when $\alpha = 60^\circ$.

Comparing Fig. 8(b) with Fig. 9(b) for $\chi = 0^\circ$, it can be seen that the maximum frequency of the in-plane modes propagating in this direction decreases as α decreases, which may be due to the softening of the interaction in the x -direction as α decreases. The maximum frequency of the modes also varies with χ for the anisotropic case shown in Fig. 9. Here the maximum frequency of the in-plane longitudinal (transverse) mode decreases (increases) as χ increases. This effect was shown also in Fig. 5 of our previous paper [16] for a purely 2D system with the same parameters. As suggested in the latter paper, owing to the reduced inter-grain spacing in

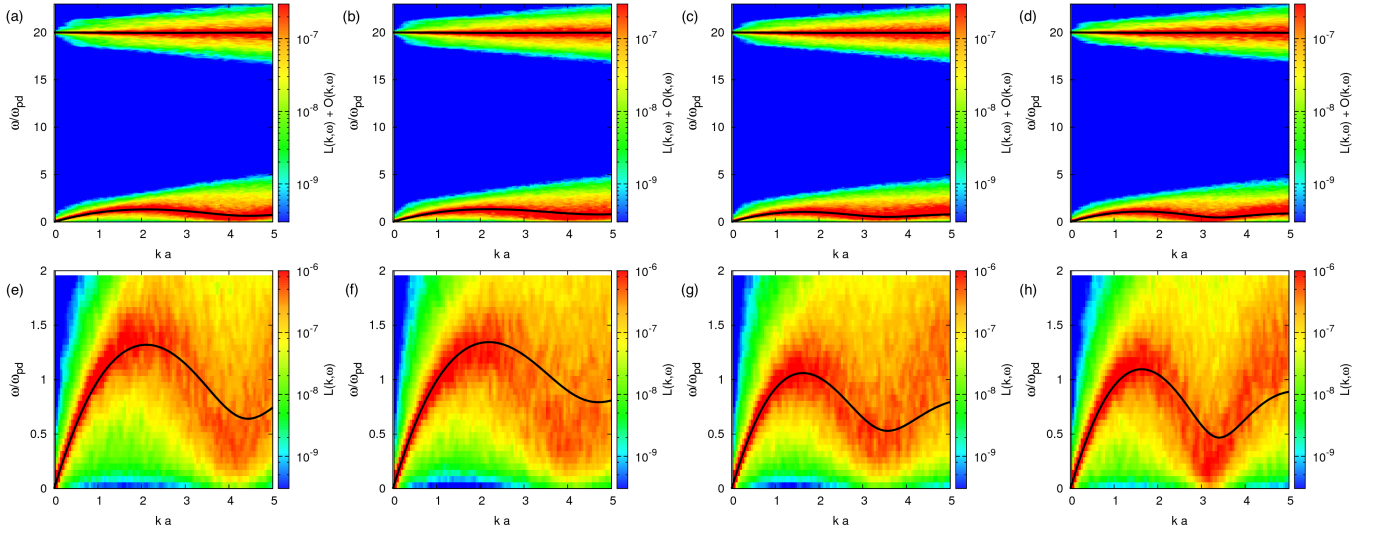


FIG. 9. (Color online) Wave dispersions for the in-plane longitudinal and out-of-plane transverse modes at several angles of propagation for a system in a strong trap (cf. Fig. 3) with parameters $\Gamma = 25$, $\kappa = 1$, $\alpha = 60^\circ$, trap frequency $\omega_t = 20\omega_{pd}$ and $\eta = 1$. The color maps in (a-d) are the in-plane longitudinal and out-of-plane transverse fluctuation spectra generated by the simulations, and the curves are the QLCA wave dispersion relations for the corresponding modes obtained from eq. (7) as a function of ka for these parameters. The color maps in (e-h) are the in-plane longitudinal fluctuation spectra, and the curves are the QLCA dispersion relations for the corresponding modes. Propagation angles $\chi = 0^\circ$ (a,e), $\chi = 30^\circ$ (b,f), $\chi = 60^\circ$ (c,g), and $\chi = 90^\circ$ (d,h).

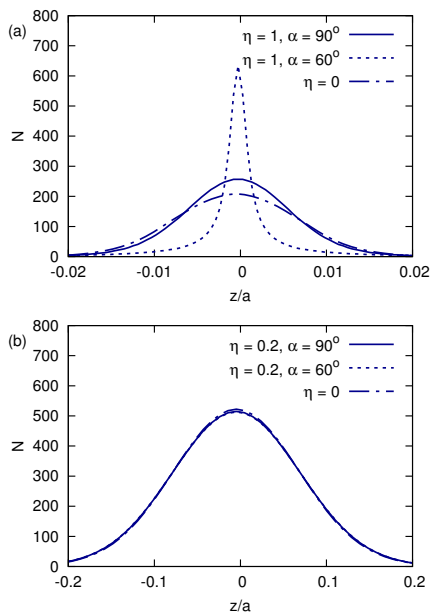


FIG. 10. (Color online) The density distribution of dust grains along the z -direction from the MD simulations, showing the effect of the magnetic field, for a system with $\Gamma = 25$, $\kappa = 1$. In (a) the trap frequency is $20\omega_{pd}$, $\eta = 1$ for $\alpha = 90^\circ$ and $\alpha = 60^\circ$, and $\eta = 0$. In (b) the trap frequency is $2\omega_{pd}$, $\eta = 0.2$ for $\alpha = 90^\circ$ and $\alpha = 60^\circ$, and $\eta = 0$. Note the dramatic sharpening of the distribution in the case of a strong trap at the tilt angle $\alpha = 60^\circ$.

the x direction and increased spacing in the y direction for $\alpha = 60^\circ$ [see e.g., Fig. 2(h)] the second derivative of the total interaction potential ϕ_{Tot} can be larger in the x direction than in the y direction. Since the restoring force acting on a particle for the longitudinal mode is proportional to the second derivative of ϕ_{Tot} along the direction of propagation, it is larger for $\chi = 0$. Thus the maximum frequency of the longitudinal mode decreases as χ increases. On the other hand, the restoring force acting on a particle for the in-plane transverse mode is proportional to the second derivative of ϕ_{Tot} in the in-plane direction transverse to the propagation direction, and would be larger for $\chi = 90^\circ$. Thus the maximum frequency of the in-plane transverse mode increases as χ increases.

Figure 10 shows the measured density profiles along the z -direction. When the trap frequency is large, as in Figs. 8 and 9, the dust layer is very thin in the z direction as shown in Figure 10(a). In this case, we would expect that the 2D and quasi-2D wave dispersions would be similar. However, we find in comparing Fig. 9 with Fig. 5 in I for a 2D system with the same parameters, there appear to be some small differences in the mode dispersion, more prominently in the $\chi = 30^\circ$ case. These differences may be related to the tendency of the trap potential to affect $g(\vec{r}, \theta)$ slightly as mentioned in relation to Fig. 2. It can be seen in Fig. 10(a) that compared to the magnetic field free case ($\eta = 0$), for $\eta \neq 0$ the

distribution sharpens, as expected, since the dipole interaction softens the repulsive force along z . This effect is even more pronounced for $\alpha = 60^\circ$ where the thickness of the dust layer is significantly smaller than for $\alpha = 90^\circ$. We speculate that this may occur because the excursion of a particle in the z direction can soften F_{Mx} more when $\alpha = 60^\circ$ than when $\alpha = 90^\circ$. This may limit the excursion in z more for $\alpha = 60^\circ$ in order that F_{Mx} remain positive. However further work is needed to investigate this effect. We note from Fig. 10(b) that when the trap frequency and η are small, it appears that the dust layer thickness has very little dependence on α .

V. SUMMARY AND DISCUSSION

We have investigated the behavior of a quasi-2D system of particles in a harmonic potential trap and interacting via Yukawa and magnetic dipole potentials. The Yukawa potential is commonly used for the isotropic interaction potential between charged dust grains (although modifications at long range have been measured in certain experiments [30]), while the magnetic dipole potential results from induced magnetic dipole moments on the grains. The model system comprises a layer of charged superparamagnetic grains in a plasma in an external, uniform magnetic field \mathbf{B} and confined by a potential in the direction perpendicular to the layer. The induced magnetic dipole moments of the grains lie along \mathbf{B} , and as the magnitude and direction of \mathbf{B} is varied and \mathbf{B} becomes tilted with respect to the layer, the interaction between the grains becomes anisotropic. There is a threshold tilt angle below which the interaction between the grains becomes attractive: the studies in this paper are confined to angles α between \mathbf{B} and the layer which are above this threshold angle. Furthermore, the studies in this paper are for confining potentials large enough to constrain the interaction between grains to remain repulsive even outside the layer: this allows the system to remain quasi-stable. By quasi-stability we mean that within the timespan of the simulation (several thousand plasma oscillation times) a “head-to-tail” collapse does not occur. (Of course one cannot guarantee that at much longer time scales such a collapse would not occur). The equilibrium 2D pair correlation functions are obtained from MD simulations, and they show more pronounced anisotropic structures as the magnetic field strength and tilt angle are increased, culminating in a stripe-like density distribution. In order to study wave propagation we apply as a theoretical approach the reformulated QLCA that can treat dipole interactions; the theoretical analysis is paralleled by MD simulations. The QLCA requires input of the pair correlation functions which are also provided by the MD simulations. The QLCA dispersion relations show reasonable agreement with the dispersion relations obtained from the fluctuation spectra generated by the MD simulations.

With the grains having small displacements in the z -

direction under the influence of a confining potential, an out-of-plane transverse mode arises, in addition to the in-plane longitudinal and transverse modes already found for a 2D system in our prior paper I. This mode has its analog in a quasi-2D Yukawa liquid [26]. The mode has a finite frequency, the trap frequency, at $k = 0$ which is determined by the strength of the confining potential. For $k \rightarrow \infty$ it goes to the Einstein frequency, which is lower than the trap frequency: the difference is due to the depolarizing effect of the grains. In general, the dispersion properties of the in-plane polarized longitudinal and transverse waves appear to be similar to those obtained for a 2D system in paper I. The wave dispersion relations depend on the angle of propagation, and the degree of anisotropy characterized by the magnetic tilt angle α and the relative strength of the magnetic dipole to Yukawa interaction characterized by η . For a fixed angle of propagation χ , both the sound speed at small k and the maximum frequency of the longitudinal in-plane mode increase as η increases, reflecting the fact that the magnitude of the total repulsive interaction potential increases as η increases, so the mode becomes harder.

The transverse out-of-plane mode can affect the polarization properties of the longitudinal in-plane mode at specific ka intervals where the frequencies of the two modes approach each other and the two modes hybridize. This can occur generally when the trap frequency is relatively low, on the order of ω_{pd} . Low trap frequencies, however, allow only systems having smaller η values, because it appears that systems with large η can only be quasi-stably attained with large confining potentials. Thus, in an experiment with large η , one might expect to observe a correspondingly large frequency difference between the out-of-plane polarized transverse wave and the two in-plane polarized modes.

We have examined finally the effect of the magnetic field on the density distribution along the direction perpendicular to the layer. Compared to the magnetic field-free distribution, at 90° tilt angle the added dipole interaction seems to result in a slight narrowing of the distribution for a system with large η and large trap frequency. However, as the tilt angle is reduced to 60° a dramatic further narrowing takes place. More work is needed to understand the details of this phenomenon.

If experiments on such 2D paramagnetic dusty plasma systems could be done, that could also have implications for the understanding the behavior of waves in other 2D systems where the particles interact via anisotropic potentials. This includes 2D electrorheological dusty plasmas [23], as well as 2D dipolar bosonic gases with tilted dipoles [24]. Because a discussion of possible experimental parameters was given in I, here we briefly summarize some points and refer the reader to I for more details. For a grain of radius R and magnetic permeability μ , the induced magnetic dipole moment is [14] $M = R^3 B(\mu - 1)/(\mu + 2)$. Then the quantity η is

$$\eta = \frac{M}{Q\lambda_D} \sim 0.03 \frac{R^2(\mu\text{m})B(\text{G})}{|\phi_s(\text{V})|\lambda_D(\mu\text{m})} \left(\frac{\mu - 1}{\mu + 2} \right).$$

From this expression, it can be surmised that in order to attain a particular value of η , the required value of B decreases as R gets larger and as the magnitude of the grains' surface potential ϕ_s gets smaller. Thus for example, in a thermal plasma with low temperature $T_e \sim T_i \sim 0.2$ eV and density $n_i \sim 4 \times 10^8$ cm $^{-3}$, and for a system of grains with $R \sim 5$ μm and $\mu = 4$, η can be ~ 0.5 for a relatively low magnetic field strength of $B \sim 100$ G. Such a system may be better suited to microgravity conditions, however, owing to challenges with levitating grains with small charge-to-mass ratios in terrestrial experiments. For a terrestrial experiment, using the same dust parameters, but assuming an rf or dc plasma with $T_e \sim 2$ eV and $n_i \sim 10^9$ cm $^{-3}$, and taking $|\phi_s| \sim 5$ V and $\lambda_D \sim \lambda_{De}$ in the sheath, we find that $\eta \sim 0.5$ implies $B \sim 2000$ G. This value of B is attainable in current experimental devices (see e.g. [12]) but there could be complications associated with magnetized ions, such as forces on the dust arising from ion flows (e.g. [31]), as well as effects on charging and shielding (e.g., [32]). In addition, while we have assumed uniform B, the agglomeration of dust grains has been observed in experiments using nonuniform B to levitate the dust [13]. In this paper we have assumed a confining potential (5) to counteract the tendency of the grains to escape from the layer.

ACKNOWLEDGMENTS

We want to acknowledge useful exchange of ideas with Hong Pan, who shared the results of his exploratory calculations on the structure of the density profile with us. This work was partially supported by NSF Grants PHY-1201978, PHY-1301856 and PHY-1105005, NASA/JPL subcontract RSA 1542954, OTKA Grant K-105476, NK-FIH Grant K-115805, and the János Bolyai Research Scholarship of the Hungarian Academy of Sciences.

Appendix: Elements of dynamical matrix

These are the elements of the dynamical matrix in the model geometry used in this paper.

$$C_{\mu\nu} = \frac{\omega_p^2}{2\pi} \int d\theta \frac{d\bar{r}}{\bar{r}^2} g(\bar{r}, \theta) [\exp(i\bar{k}\bar{r} \cos(\chi - \theta)) - 1] \Phi_{\mu\nu}.$$

Here

$$\Phi_{xx} = \exp(-\bar{\kappa}\bar{r}) [(1 + \bar{\kappa}\bar{r}) (1 - 3 \cos^2 \theta) - \cos^2 \theta \bar{\kappa}^2 \bar{r}^2] + \frac{3\eta^2}{\bar{\kappa}^2 \bar{r}^2} [1 - 5 \cos^2 \theta + \cos^2 \alpha (2 - 25 \cos^2 \theta + 35 \cos^4 \theta)],$$

$$\Phi_{yy} = \exp(-\bar{\kappa}\bar{r}) [(1 + \bar{\kappa}\bar{r}) (1 - 3 \sin^2 \theta) - \sin^2 \theta \bar{\kappa}^2 \bar{r}^2] + \frac{3\eta^2}{\bar{\kappa}^2 \bar{r}^2} [1 - 5 \sin^2 \theta - \cos^2 \alpha \cos^2 \theta (5 - 35 \sin^2 \theta)],$$

$$\begin{aligned} \Phi_{xy} = \Phi_{yx} = \\ \exp(-\bar{\kappa}\bar{r}) \left[(1 + \bar{\kappa}\bar{r}) (-3 \cos \theta \sin \theta) - \cos \theta \sin \theta \bar{\kappa}^2 \bar{r}^2 \right] \\ + \frac{3\eta^2}{\bar{\kappa}^2 \bar{r}^2} \left[\cos \theta \sin \theta (-5 - \cos^2 \alpha (10 - 35 \cos^2 \theta)) \right], \end{aligned}$$

$$\begin{aligned} \Phi_{zz} = \exp(-\bar{\kappa}\bar{r}) \left[(1 + \bar{\kappa}\bar{r}) \right] \\ + \frac{3\eta^2}{\bar{\kappa}^2 \bar{r}^2} \left[1 - 5 \cos^2 \alpha \cos^2 \theta + 2 \sin^2 \alpha \right], \end{aligned}$$

$$\Phi_{zx} = \Phi_{xz} = \frac{3\eta^2}{\bar{\kappa}^2 \bar{r}^2} \left[\sin \alpha \cos \alpha (2 - 10 \cos^2 \theta) \right],$$

$$\Phi_{zy} = \Phi_{yz} = \frac{3\eta^2}{\bar{\kappa}^2 \bar{r}^2} \left[-10 \sin \alpha \cos \alpha \sin \theta \cos \theta \right].$$

-
- [1] M. Bonitz, C. Henning and D. Block, *Rep. Prog. Phys.* **73**, 066501 (2010).
- [2] V. E. Fortov, A. V. Ivlev, S. A. Khrapak, A. G. Khrapak and G. E. Morfill, *Phys. Rep.* **421**, 1 (2005).
- [3] P. K. Shukla and B. Eliasson, *Rev. Mod. Phys.* **81**, 25 (2009).
- [4] K. O. Menzel, O. Arp and A. Piel, *Phys. Rev. Lett.* **104**, 235002 (2010).
- [5] M. Schwabe, M. Rubin-Zuzic, S. Zhdanov, H. M. Thomas and G. E. Morfill, *Phys. Rev. Lett.* **99**, 095002 (2007).
- [6] E. Thomas, Jr., *Phys. Plasmas* **17**, 043701 (2010).
- [7] M. Himpel, T. Bockwolddt, C. Killer, K. O. Menzel, A. Piel and A. Melzer, *Phys. Plasmas* **21**, 033703 (2014).
- [8] V. E. Fortov, O. F. Petrov, V. I. Molotkov, M. Y. Poustylnik, V. M. Torchinsky, A. G. Khrapak and A. V. Chernyshov, *Phys. Rev. E* **69**, 016402 (2004).
- [9] D. V. Tkachenko, T. E. Sheridan and V. R. Misko, *Phys. Plasmas* **18**, 103709 (2011).
- [10] T. M. Flanagan and J. Goree, *Phys. Plasmas* **17**, 123702 (2010).
- [11] R. L. Merlino, J. R. Heinrich, S.-H. Hyun and J. K. Meyer, *Phys. Plasmas* **19**, 057301 (2012).
- [12] E. Thomas, Jr., R. L. Merlino and M. Rosenberg, *Plasma Phys. Control. Fusion* **54**, 124034 (2012).
- [13] D. Samsonov, S. Zhdanov, G. Morfill and V. Steinberg, *New J. Phys.* **5**, 24.1 (2003).
- [14] V. V. Yaroshenko, G. E. Morfill, D. Samsonov and S. V. Vladimirov, *IEEE Trans. Plasma Sci.* **32**, 675 (2004).
- [15] P. Hartmann, M. Rosenberg, G. J. Kalman and Z. Donko, *Phys. Rev. E* **84**, 016409 (2011).
- [16] P. Hartmann, Z. Donko, M. Rosenberg and G. J. Kalman, *Phys. Rev. E* **89**, 043102 (2014).
- [17] J. D. Feldmann, G. J. Kalman, P. Hartmann and M. Rosenberg, *Phys. Rev. Lett.* **100**, 085001 (2008).
- [18] Z. Donko, P. Hartmann and G. J. Kalman, *Phys. Rev. E* **69**, 065401(R) (2004).
- [19] K. I. Golden, G. J. Kalman, Z. Donko and P. Hartmann, *Phys. Rev. B* **78**, 045304 (2008); **78**, 239905(E) (2008).
- [20] K. I. Golden, G. J. Kalman, Z. Donko and P. Hartmann, *J. Phys. A: Math. Theor.* **42**, 214017 (2009).
- [21] K. I. Golden, G. J. Kalman, P. Hartmann and Z. Donko, *Phys. Rev. E* **82**, 036402 (2010).
- [22] A. V. Ivlev et al., *IEEE Trans. Plasma Sci.* **38**, 733 (2010).
- [23] R. Kompaneets, G. E. Morfill and A. V. Ivlev, *Phys. Plasmas* **16**, 043705 (2009).
- [24] A. Macia, F. Mazzanti and J. Boronat, *Eur. Phys. J. D* **66**, 301 (2012); A. Macia, D. Hufnagl, F. Mazzanti, J. Boronat and R. E. Zillich, *Phys. Rev. Lett.* **109**, 235307 (2012).
- [25] N. Hoffman, C. N. Likos and H. Lowen, *Molec. Phys.* **105**, 1849 (2007).
- [26] Z. Donko, G. J. Kalman and P. Hartmann, *J. Phys. Condens. Mat.* **20**, 413101 (2008).
- [27] K. I. Golden and G. J. Kalman, *Phys. Plasmas* **7**, 14 (2000).
- [28] P. Hartmann, Z. Donko, G. J. Kalman, S. Kyrkos, M. Rosenberg and P. M. Bakshi, *IEEE Trans. Plasma Sci.* **35**, 337 (2007).
- [29] S. Zhdanov, S. Nunomura, D. Samsonov and G. Morfill, *Phys. Rev. E* **68**, 035401 (2003).
- [30] O. S. Vaulina, E. A. Lisin, A. V. Gavrikov, O. F. Petrov and V. E. Fortov, *Phys. Rev. Lett.* **103**, 035003 (2009).
- [31] U. Konopka, D. Samsonov, A. V. Ivlev, J. Goree, V. Steinberg and G. E. Morfill, *Phys. Rev. E* **61**, 1890 (2000).
- [32] V. N. Tsytovich, N. Sato and G. E. Morfill, *New J. Phys.* **5**, 43 (2003).